2019

Mechanochemically Synthesized Cobalt Oxide-Based Particles for the Reduction of Nitrophenols and Impacting Factors to its Mechanism

Lorianne R. Shultz
University of Central Florida

MECHANOCHEMICALLY SYNTHESIZED COBALT OXIDE-BASED PARTICLES FOR THE REDUCTION OF NITROPHENOLS AND IMPACTING FACTORS TO ITS MECHANISM

by

LORIANNE REBECCA SHULTZ

A thesis submitted in partial fulfillment of the requirements
for Honors in the Major
Department of Chemistry
in the College of Sciences
at the University of Central Florida
Orlando, Florida

Spring Term
2019

Major Professor: Titel Jurca

ABSTRACT

Mechanochemically synthesized cobalt oxide-based particles are employed for the catalytic reduction of 4-nitrophenol (4NP), a toxic water contaminant. This reduction produces 4-aminophenol (4AP), a less toxic, pharmaceutical precursor for drugs such as paracetamol. The indicated reduction has been completed previously using noble metals and/or catalysts requiring extensive solvent use, and time as part of their preparation. The cost and synthesis of these noble metal catalysts hinders the sustainable broad scale application as an environmental remediation solution. The catalyst synthesis explored in this study utilizes the green chemistry technique of vibratory ball-milling and annealing cobalt oxide-based particles at different temperatures, producing unique agglomerates with differing surface structure and catalytic properties. Additional investigation into the mechanism through temperature, pH, and change in pressure over the reaction is completed. Further analysis shows that these catalysts are efficient for the reduction of 4-amino-3-nitrophenol and 2-amino-5-nitrophenol with unique catalytic rates. Finally, it is found that the application of this reduction in a flow process has potential for use on a broader scale.

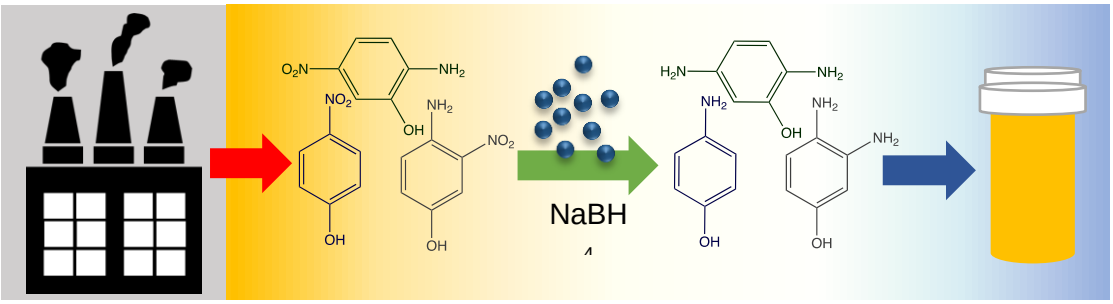

Figure 1: Overview of Research Importance

ACKNOWLEDGEMENTS

I am deeply grateful to my adviser, Dr. Titel Jurca, for his enduring mentorship, investing in me, and without whom none of this research would be possible. Thank you to my committee members, Dr. Melanie Beazley and Dr. Humberto Campins for their time and constant support. I only hope to be half as prolific as them. A special thanks to my graduate student mentor, Thomas Shaw, for his insightful suggestions, answering a thousand questions, and helping with the synthesis of the particles studied in this thesis. Many thanks to Bryan McCullough and Dr. Matthieu Baudelet for the characterization of these particles through Raman Spectroscopy and SEM. I am grateful to Wesley Newsome for introducing me to physisorption and pXRD characterization techniques and to Dr. Fernando Uribe-Romo and Wesley for this characterization on the particles studied. I am humbled and grateful to the entire Jurca Lab group for helpful discussions and willingness to troubleshoot problems when they arose. Finally, I cannot begin to express my thanks to my loving parents, Cassie, Sadie, Eric, and Roger for their incredible patience and unwavering encouragement.

Table of Contents

Table of Figures

LIST OF ABBREVIATIONS

BET	Brunauer-Emmett-Teller
DIW	Deionized Water
EDX	Energy Dispersive X-Ray
FTIR	Fourier Transform Infrared Spectroscopy
pXRD	Powder X-Ray Diffraction
SEM	Scanning Electron Microscopy
UV-Vis	Ultra Violet and Visible
$Co(OH)_2$	Cobalt Hydroxide
CoO(OH)	Cobalt Oxyhydroxide
Co_3O_4	Cobalt Oxide Spinel Species
Co_{100}	Cobalt Particles Calcinated at 100 ˚C
Co_{350}	Cobalt Particles Calcinated at 350 ˚C
Co_{600}	Cobalt Particles Calcinated at 600 ˚C
$NaBH_4$	Sodium Borohydride
4AP	4-Aminophenol
4AP*	4-Aminophenolate
2A5NP	2-Amino-5-Nitrophenol
4A3NP	4-Amino-3-Nitrophenol
4NP	4-Nitrophenol
4NP*	4-Nitrophenolate

CHAPTER 1: INTRODUCTION

1.1: Introduction to the Topic

4-Nitrophenol (4NP) is a nuisance water contaminant from numerous industrial processes such as the steel, rubber, electronic, textile, explosive and pesticide industries. This compound is also made through photochemical processes when nitrobenzene, toluene, and bromobenzene react with nitric oxides in the air. In addition, this toxic chemical is produced by hydrolysis and biodegradation of sulfur or phosphorous compounds to nitrophenol[1,2]. It has been labeled as one of America's top priority pollutants by the Environmental Protection Agency[3] due to its carcinogenetic and mutagenic abilities as well as its connection with liver disease[1] in concentrations as small as 1 ng L^{-1}, and as its ability to enact cyanosis and methemoglobinemia in humans[2].

The reduction of 4NP, which is the conversion of the nitro-functional group into an amine-functional group, produces 4-aminophenol (4AP). This compound is significantly less toxic and is a vital pharmaceutical precursor for antipyretic and analgesic drugs such as paracetamol (acetaminophen) and acetanilide, in addition to its use as a component in other industrial processes, such as photographic developer preparation[2,4]. The reduction process, however, requires a source of hydrogen as well as a catalyst to proceed.

1.2: Literature Review

1.2.1: Reduction of Nitrophenol Background

The reduction of 4NP to 4AP is a six-electron transfer process with a 44 KJ mol^{-1} activation energy[4]. Due to the activation energy being steep, this reduction requires the use of a catalyst to aid in the production of an active hydrogen source through hydrolysis of another base or acid. Typically sodium borohydride is used due to its stability at a wide range of pH[5]. For this process, the most commonly used catalysts are gold[6], silver[7], platinum[8,9], and palladium[9,10] based nanoparticles. There are several proposed mechanisms in which heterogeneous catalytic reduction of nitrophenol is completed. Those proposed are the Langmuir-Hinshelwood model, Eley-Rideal model, superconductor model, and photocatalytic model[4]. The model corroborated the most by researchers is the Langmuir-Hinshelwood model[11].

The Langmuir-Hinshelwood model proposes that both reactants participating in the catalytic reaction must be adsorbed onto the catalyst in a reversible manner before the reaction takes place. Subsequently, they are desorbed post reaction. For example, in 4-nitrophenol reduction, 4NP would adsorb onto the catalyst, likely through its oxygen atoms in the nitro-group. The borohydride, from the sodium borohydride salt, would be adsorbed onto the catalyst, and the interaction of the borohydride and catalyst would provide the hydrogen necessary for the reduction of 4NP to take place[4,11,12]. When the d-band of the metal and 4NP interact, the electron energy states split, causing the bonding levels to fall lower than the Fermi level and the antibonding levels to become more inhabited. This weakens the adsorption strength thus easing

the desorption step after the reduction[4]. Proposed intermediates for 4NP reduction are 4-hydroxyaminophenol and 4-nitrosophenol[4,9].

Assuming the Langmuir-Hinshelwood model holds true, kinetics can be extracted from experimental concentrations and adsorption constants using the Langmuir-Hinshelwood equation shown in **Equation 1**[12].

Equation 1: Langmuir-Hinshelwood Kinetics Equation

$$k_{app} = \frac{k * S * K_{4NP}^{n}[4NP]^{n-1}\left(K_{BH_4^-}[BH_4^-]\right)^{m}}{\{1 + K_{4NP}[4NP\}^{n} + (K_{BH_4^-}[BH_4^-]^{m}\}^{2}}$$

Here k_{app} is the surface rate constant, S is the total catalyst surface area, K_{4NP} and $K_{BH_4^-}$ are the adsorption constants, and m and n are the Freundlich exponents that are material dependent on the heterogeneity of the catalyst's surface[12].

In the presence of excess base and sufficient catalyst, as well as assuming that the borohydride group desorbs irreversibly and thus does not impact that reaction rate, and that the reactants' adsorption and desorption steps are not rate determining, this kinetic expression can be simplified to a pseudo-first order reaction rate[11]. Then, the rate determining step is the conversion of 4NP into 4-hydroxyaminophenol[4]. This rate is related to the concentration of the species of 4NP and 4-hydroxyaminophenol. Due to 4NP being a light yellow color and 4AP being colorless, this reaction can be monitored through Ultra Violet-Visible (UV-Vis) spectroscopy. The relation of these measurements and the rate is evident in the pseudo-first order reaction rate law in **Equation 2** below[11].

Equation 2: Pseudo-First Order Rate Equation

$$-k_{app}(t - t_0) = \ln\left(\frac{C_t}{C_0}\right) = \ln\left(\frac{A_t}{A_0}\right)$$

In which C_t is the concentration at time t, C_0 is the initial concentration, and k_{app} is the apparent kinetic rate. The as-proposed Langmuir-Hinshelwood mechanism is shown in **Figure 2** for better understanding.

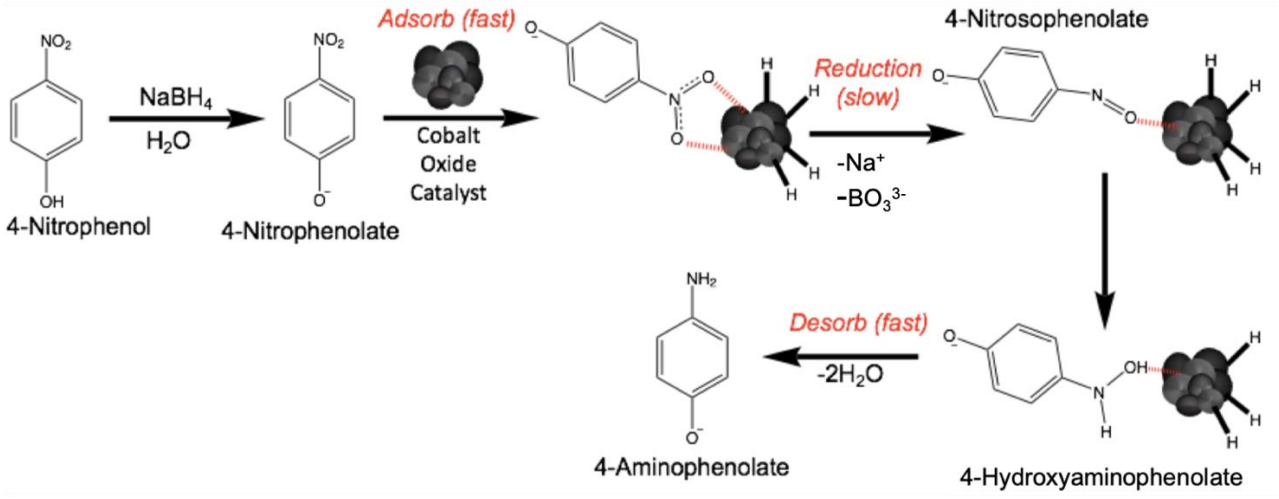

Figure 2: Langmuir-Hinshelwood Mechanism of 4NP Reduction

The kinetic rate is related to the catalytic activity and can thus be used in the comparison of different catalysts. The rate is characteristically proportional to the total surface of the catalyst, the kinetic rate constant K, and the adsorptions of 4NP and borohydride onto the catalyst[4]. It is important to note that there is usually an induction period prior to the reduction step, typically labeled t_0. This is common for heterogeneous catalysts when they are placed in solution as their surface may undergo a restructuring step. This induction time usually decreases with recyclability

as Mei et al. reported that once the catalyst was utilized for one trial, the induction time of the studied catalysts decreased significantly[9].

1.2.2: History of Catalysts

Properties of primary focus for heterogeneous catalysts are surface area, porosity, facet selection, atom affinity, and structure of the catalyst[4]. There have been a number of nanoparticle catalysts examined for the reduction of nitrophenol including noble metals, bimetallic particles, and metal oxides.

Gold nanoparticles have been a major focus in the reduction of nitrophenols as gold has recently been found to have catalytic properties. Shah et al. synthesized gold nanoparticles by a sorption-reduction method that were then used to reduce with yields above 80 % 4-nitrophneol, nitrobenzene, 4-nitroaniline, 2-nitroaniline, 4-bromonitrobenzene, 4-nitrobenzaldehyde, and 4-nitrobenzoic[6]. In addition to gold, other noble metal catalysts have proved highly efficient for this reduction such as silver, platinum, and palladium-based nanoparticles. Dolatkhah et al. produced polymer-based silver nanoparticles for the reduction of nitrophenol. 4NP was reduced almost 17 times faster than 4NP reduction with pure silver nanopartles[7]. Platinum, a generally more active catalyst than silver, also proved efficient in this reduction. Pandey et al. produced platinum nanoparticles supported on guar gum, a fine powder produced from seeds, in an attempt to provide a sustainable support for the platinum catalyst[8]. These supported particles (50 µL of 2.5 mM) reduced 0.1 x 10^{-3} M 4NP by a noteworthy 97 % in a matter of 320 seconds[8].

Mei et al. also produced platinum nanoparticles, however, they were supported on spherical polyelectrolyte brushes which acted as carriers of the substrate to the active sites. These catalysts had high colloidal stability even at elevated temperatures[9].

Palladium, compared to platinum, has increased catalytic rates due to its high surface to volume ratio[9]. Gopalakrishnan et al. produced palladium nanoparticles in a green method via bioreducing Pd^{2+} into Pd^{0} by the use of milk thistle seeds. These nanoparticles worked well for the reduction of 4-nitrophenol, providing an eco-friendly method for producing a noble metal catalyst[10].To end this brief summary of noble metal nanoparticle catalysts, Gopiraman et al. synthesized gold, silver, and nickel nanoparticles supported on cellulose that proved competent for 4-nitrophenol reduction as well as 2-nitrophenol reduction[13]. This reaction was able to reduce 0.800 mmol 4NP with less than 1 mg of catalyst in less than 5 min and at a yield of 100 %[13].

As stated prior, bimetallic catalysts have also been utilized for the reduction of nitrophenols. One such example of this is Pt-Ni bimetallic nanoparticles synthesized by Ghosh et al. These catalysts were suitable for the reduction of 4-nitrophenol, 2-nitrophenol, and 4-nitroaniline with decreasing rates respectively[14]. 4NP reduction rate increased as temperature was increased. Moreover, it was found that an increase in the nickel:platinum ratio correspondingly increased the rate for reduction[13]. This is explained through electronegativity. Because nickel has a lower electronegativity than platinum, it is a better electron donor and thus provides electron

enrichment to the platinum surface aiding in the reduction of the substrate once adsorbed on the surface[14].

Metal oxide-based nanoparticles have also been used for the reduction of nitrophenol. This subcategory of catalysts is the main focus of this thesis proposal, specifically cobalt oxide-based particles, due to its cost-effectiveness and limited research. Gopel and coworkers have previously reported transition metal oxide catalysts for 4NP reduction. Prior to this publication, TiO_2, V_2O_2, Cr_2O_3, MnO_2, and ZnO were established as inactive for nitrophenol reduction[15]. In general, d^n (n = 5-9) are active but d^0, d^3, and d^{10} were said to be inactive for nitroarene reductions. Contrarily, CuO, Co_3O_4, Fe_2O_3 and NiO catalysts produced by Gopal et al. were active for this reduction[15]. In a 1 mM solution of 4NP, 100 mg of the first three respective metal oxide nanoparticles catalyzed the reduction 100 % in a timeframe between 40 and 130 seconds with increasing times respectively, and thus decreasing rates[15]. NiO had a much lower activity, completing the reduction in 16-20 min. The publication concluded that the catalytic rates are related to the semi-conducting band gap values for each of the metal oxide nanoparticles where the smaller the band gap (eV) the more efficient the catalyst[15]. CuO and Co_3O_4 were active for increased concentrations of 4NP, at 5 mM, as well as decreased concentrations of $NaBH_4$, proving prospective use in bulk reductions of this pollutant[15]. The publication concluded that modifying these catalysts into supported nanoform would produce effective catalysts for 4NP reduction[15].

Following this, Meijboom and coworkers published a broad study on cobalt oxide-based nanoparticles produced in a surfactant micelle method and calcinated at different temperatures[12]. This surfactant micelle technique is a lengthy method involving the dissolution of cobalt nitrate hexahydrate in a solution of pluronic123 (a symmetric triblock copolymer), nitric acid, and 1-butanol. Once stirred for 30 min and oven dried at 120 ˚C for 3.5 hr, the red powder was washed with ethanol and calcinated at 150 ˚C for 12 hr. Separated into five allotments, each section was heated 100 ˚C higher than the previous for 1 hr, producing Co-150, Co-250, Co-350, Co-450, and Co-550[12]. The data indicated that the temperature of calcination is proportional to the pore size and inversely proportional to the surface area and catalytic rate of reduction.

Liu et al. produced cobalt oxide composite hollow polyhedrons (Co_3O_4/CoP) which were effective for 4NP reduction with yields of almost 100 % in roughly 3 min[5]. The synthesis process of these were rather involved starting with a solution of cobalt nitrate hexahydrate, 2-methylimidazole, and methanol, stirring for 30 min, letting sit for 24 hr, and oven drying at 60 ˚C for 12 hr. Finally, they were annealed at 300 ˚C for 2 hr[5]. Unique from the other cobalt oxide catalyst publications, Liu et al. studied the impact of pH on the system. Liu et al. reported an increase in activity with an increase of pH until a pH of 10. This is likely related to the stability of sodium borohydride which increases from pH 7 to pH 14, with pH 14 being optimal[5].

1.3: Intent

Previously utilized catalysts for the reduction of 4-nitrophenol have been either synthesized from expensive noble metals, or through extensive wet chemical techniques thus making the remediation of this water pollutant unsustainable. A method to synthesize cobalt oxide-based particles from a mechanochemical method via vibratory ball-milling is therefore proposed. This method is a one-pot, solid-state process that could provide a sustainable route for the environmental reduction of a priority pollutant.

Additional study of the catalysts produced involves the reduction of uniquely substituted nitrophenols. Historically, the reduction of 4NP has been considered the model reaction for benchmarking the reduction activity of heterogeneous catalysts. This reaction scheme, while beneficial for preliminary data, paints an incomplete picture when comparing catalytic rates for nanoparticle catalysts due to the fact that catalytic activity is impacted by the presence of substituents on 4-nitrophenol. To provide a more thorough investigation on these nanoparticle catalysts, the reduction of three different substituted nitrophenols is investigated, specifically 4-nitrophenol, 4-amino-3-nitrophenol, and 2-amino-5-nitrophenol (shown in **Figure 3)**, and the catalytic activity of the cobalt oxide-based particles will be compared for each reduction.

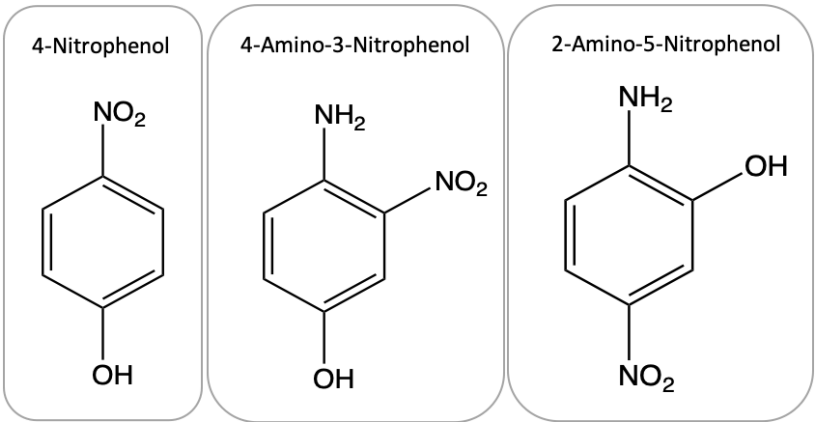

Figure 3: Structures of the Focused Substituents for This Study

Furthermore, a study on the pH and temperature in the system during the reduction will help give an enhanced understanding of the mechanism and impact of all these variables which have been mostly ignored in other reported studies. Additionally, an experiment measuring the increase in pressure during the reduction in a sealed vial will provide information on how many moles of hydrogen gas is produced in this system. Ultimately, application of this reduction in a flow process will provide a proof of concept model for the application of this process on a broader scale.

CHAPTER 2: METHODOLOGY

The first part of the process entailed the synthesis and characterization of the cobalt oxide-based particles through vibratory ball-milling. Cobalt (II) chloride hexahydrate (4.2 mmol) and potassium hydroxide (KOH) in excess (89 mmol) was added to a tungsten carbide (WC) vial with two WC ball bearings inside. This vial was sealed and placed in a SPEX 8000 vibratory mill which vibrated the vial for 2 hours (**Figure 4**). The collisions of the bearings with the vial wall and with each other provides elastic deformation, plastic deformation, and ultimately chemical reactions depending on the energy supplied (**Figure 5**). This method provided a solvent-free approach to synthesizing cobalt-oxide particles. Following this, the dark brown powder was filtered through a medium glass filter with 100 mL of DIW to separate out the large particulates and centrifuged at 3500 rpm for 3 min to collect the product. This solid product was placed in a vacuum oven at 100˚ C for 4 hours to dry. This yielded 387 mg of dark brown/black powder. The product was split into three allotments. The first allotment was left as is and is called Co_{100}, the second allotment was heated to 350 ˚C (110 ˚C h^{-1} for 3 hr, hold 2 h at 350 ˚C) which is labeled Co_{350}, and the last allotment was heated to 600 ˚C (110 ˚C h^{-1} for 5 hr, hold 2 hr at 600 ˚C) which is called Co_{600}. These three different particles were sealed and held in a desiccator when not in use.

These particles were thoroughly characterized through Fourier transform infrared spectroscopy (FTIR) and UV-Vis spectrophotometry in the Jurca Laboratory at the University of Central Florida as well as by Raman spectroscopy, powder x-ray diffractometry (pXRD), scanning electron

microscopy (SEM), energy-dispersive X-ray spectroscopy (EDX), and accelerated surface area and porosimetry system of obtain adsorption isotherms for Brunauer-Emmett-Teller (BET) surface area calculation, all through collaboration.

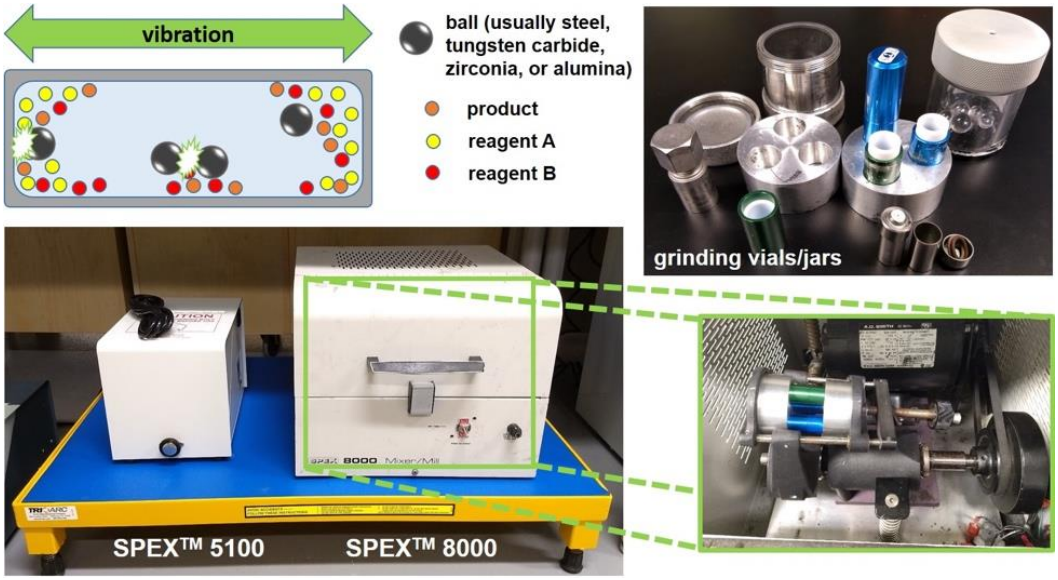

Figure 4: Vibratory Ball-Mill Set-Up

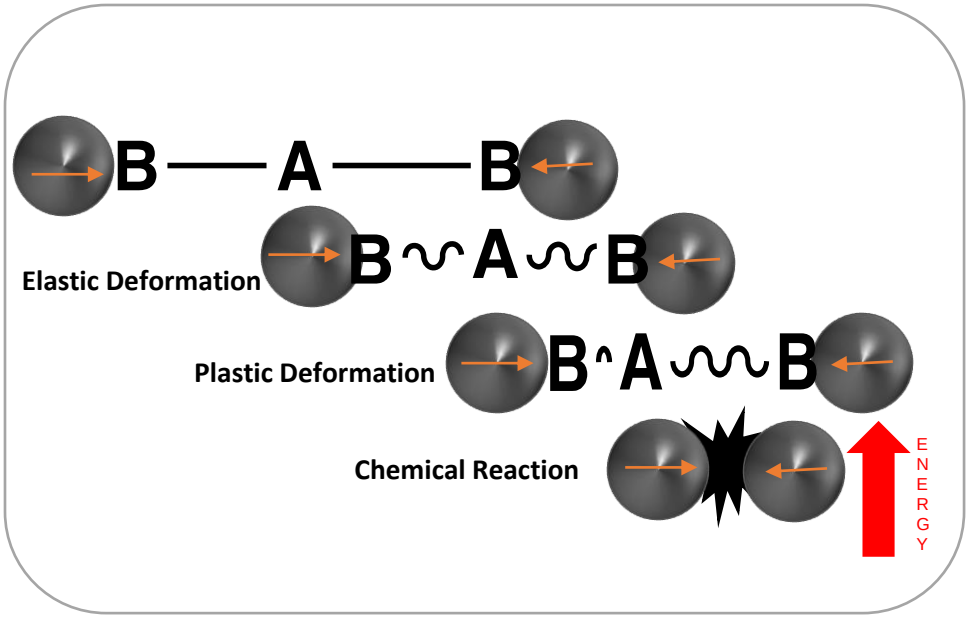

Figure 5: Ball-Milling Outcomes

Catalytic activity for each of the three species were determined and compared for the reduction of 4-nitrophenol, 4-amino-3-nitrophenol, and 2-amino-5-nitrophenol. This was completed through monitoring the reaction by UV-Vis spectrophotometry and extracting the kinetic rate from plotting **Equation 2**.

To better understand the mechanism of the cobalt-oxide based catalyst, the pH and temperature were monitored throughout the reduction concurrently using a pH probe and temperature probe. Additionally, the amount of hydrogen gas produced in this reaction was determined by monitoring the change in pressure over the entire reaction and applying the Van der Waals equation for real gases (**Equation 3**).

Equation 3: Van der Waals Equation

$$\left(\mathrm{P} + \frac{\mathrm{n}^2\mathrm{a}}{\mathrm{V}^2}\right)(\mathrm{V} - \mathrm{nb}) = \mathrm{nRT}$$

Here, P is the pressure, V is the volume of the system, R is the ideal gas constant, T is the temperature, n is the number of moles, and a and b are the gas-dependent constants. These experiments aided in a better understanding the impact of each of these factors and their relation to catalytic activity and mechanism.

Finally, presentation of a flow process was completed through a proof-of-concept method. A syringe was loaded with sodium borohydride ($NaBH_4$), deionized water (DIW), and 4NP, with

ratios identical to the catalysis trials. The syringe was placed on a syringe pump and the solution flowed through a filter loaded with the synthesized cobalt oxide-based particles. The absorption spectrum of the collected solution was obtained to ensure the completion of the reduction by this method.

CHAPTER 3: RESULTS

3.1: Cobalt Oxide-Based Particles' Characterization

The cobalt oxide-based particles were characterized through SEM and showed amorphous agglomeration of nano-to-micron sized particles (**Figure 6**), much larger than the nanoparticles discussed in the literature review. These particles were similar to those of $Co(OH)_2$ (cobalt hydroxide), CoO(OH) (cobalt oxyhydroxide), and Co_3O_4 (cobalt oxide spinel structure)[15,16,17]. EDX confirms cobalt as the predominant species as well as the presence of potassium left-over from the ball-milling synthesis with potassium hydroxide. This instrumentation, however, does not lend information about the relative amounts of each hydroxide and oxide species. For this, further characterization using Raman spectroscopy, UV-Vis spectrophotometry, FTIR, and pXRD are utilized.

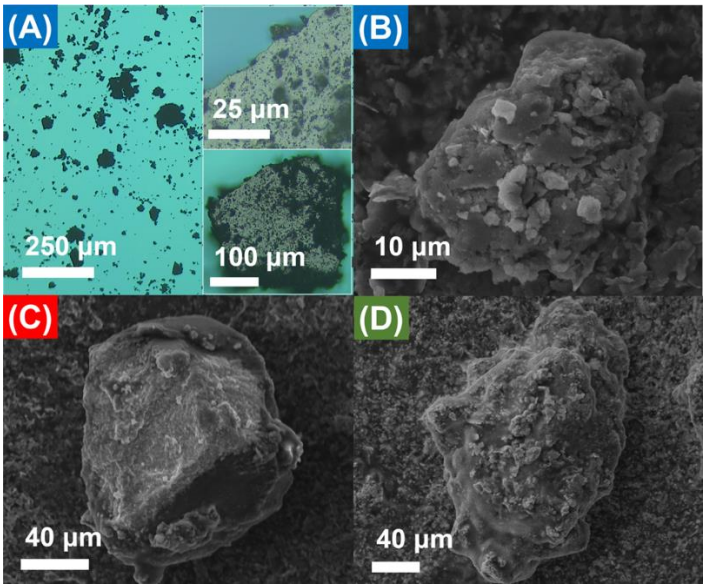

Figure 6: SEM Images of Co_{100} (B), Co_{350} (C), and Co_{600} (D)

The Raman spectroscopy of the Co_{100} species revealed peaks at 198, 491, 528, 624, and 694cm^{-1} which correspond to the F_{2g}, E_g, F_{2g}, F_{2g}, and A_{1g} modes of Co_3O_4 (**Figure 7A**)[18]. Additionally, there

are broadened peaks at 500 cm^{-1} which is characteristic of cobalt hydroxide's and cobalt oxyhydroxide's E_g and A_{2u} modes in conjunction with a peak around 600 cm^{-1} which is characteristic to the A_{1g} and E_g modes of these species[18,19,20]. In comparing the Co_{350} and Co_{600} particles to the Co_{100} species, the broad peaks around 500 and 600 cm^{-1} disappear the higher the catalyst is calcinated while the peaks corresponding to the Co_3O_4 spinel species becomes more marked. Broad features in the region of 130 to 300 cm^{-1} are credited to residual KOH in the particles.

The FTIR displays peaks at 551 cm^{-1} (v_1) and 659 cm^{-1} (v_2) (**Figure 7B**). The v_1 peak is expected to come from the Co^{3+}-O in Co_3O_4, CoO(OH), and $Co(OH)_2$ whereas v_2 is indicative of the vibration of Co^{2+}-O in Co_3O_4. As seen, the more the species was calcinated, the more intense v_2 becomes and less intense v_1 becomes. Extra peaks are attributed to surface water at 1614 cm^{-1} and carboxylates appearing also at 1614 cm^{-1} and 1360 cm^{-1} which likely formed while handling and from storage. Broad peaks on the FTIR are attributed to residual KOH in the system, however the direct characterization of these peaks is difficult due to the complexity of KOH.

It is clear that the UV-Vis spectra of Co_{100} in DIW shows intensities at λ_{max} = 390 nm (**Figure 7C**) which is indicative of CoO(OH)[21,22]. Additionally, there is poorly defined absorbance through the 800 nm measured, which is credited to the Co_3O_4 species per the Raman and FTIR characterization. The spectra of Co_{350} and Co_{600} reveal a decrease in λ_{max} = 390 nm peak and an

appearance of peaks at λ_{max} = 430 nm and 740 nm which is characteristic of the ligand-metal charge transfer events O -> Co^{2+} and O -> Co^{3+} in the Co_3O_4 species[23].

The pXRD of Co_{100} shows peaks mainly associated with $Co(OH)_2$ and CoO(OH) (**Figure 7D**). From Co_{100} to Co_{350}, peaks corresponding to the nanocrystalline Co_3O_4 spinel species are present while the $Co(OH)_2$ is only in low quantities. From Co_{350} to Co_{600}, the $Co(OH)_2$ species' peaks disappear leaving only sharp peaks for Co_3O_4. In conclusion, it is evident that the higher the cobalt particles are calcinated, the more predominant the Co_3O_4 species becomes and the less of the $Co(OH)_2$ and CoO(OH) species present.

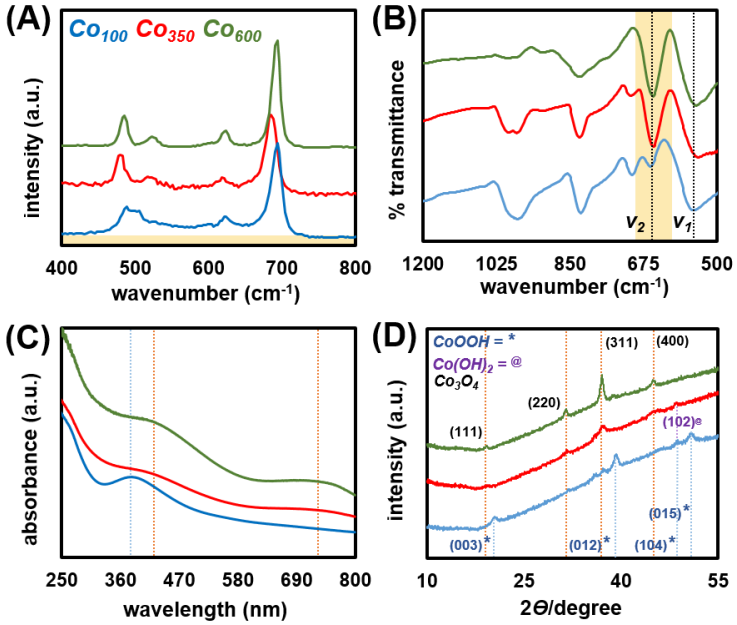

Figure 7: Raman Spectroscopy (A), FTIR (B), UV-Vis (C), and pXRD (D) Spectra

In order to reveal the surface area of these particles, N_2 gas adsorption isotherms were obtained at 77 K. These isotherms can be utilized in conjunction with the Brunauer-Emmet-Teller (BET)

model (**Figure 8**) in the low-pressure region to calculate surface area. The BET surface area[24] of Co_{100} is 21.75 m^2g^{-1}, that of Co_{350} is 28.48 m^2g^{-1}, and that of Co_{600} is 10.38 m^2g^{-1}.

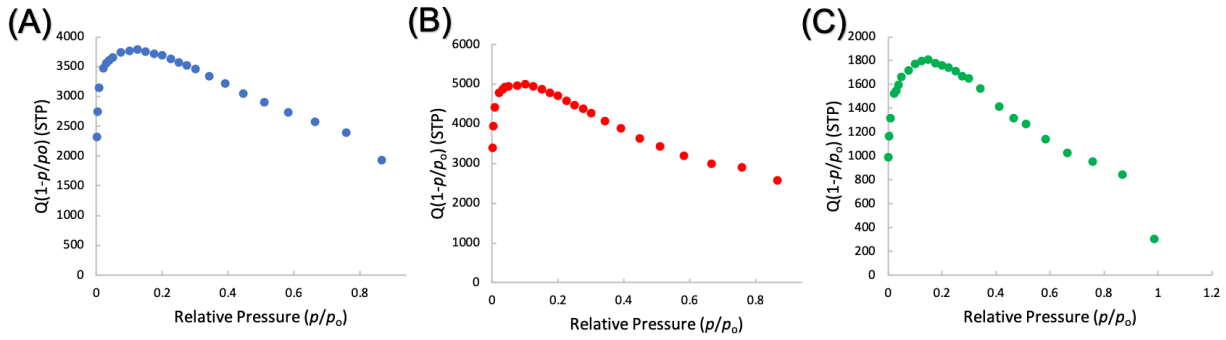

Figure 8: Rouquerol Plots of Co_{100} (A), Co_{350} (B), and Co_{600} (C)

3.2: Catalysis Trials and Mechanistic Study

Each cobalt oxide-based particle species was tested for the reduction of 4NP. This was studied in ambient conditions using UV-Vis spectrophotometry as stated in the Methodology Chapter. In order to test this, a UV-Vis spectrum of 0.39 µmol of 4NP and 0.2 mmol of $NaBH_4$ in 3 mL of DIW was obtained in a 1 cm quartz cuvette. An initial red shift of the 4NP from λ_{max} = 317 nm to λ_{max} = 400 nm in the presence of $NaBH_4$ (**Figure 9A**) indicates the deprotonation of the alcohol functional group becoming 4-nitrophenolate (4NP*). After the initial scan of this solution, 1 mg of the studied particle catalyst was placed in the system, stirred for ~2 sec, and the spectra was recorded at 2 min intervals (**Figure 9B**). The degradation of at λ_{max} = 400 nm was then used to obtain kinetics for each reduction. The fully reduced spectrum displays a complete disappearance at λ_{max} = 400 nm and the appearance of a at λ_{max} = 310 nm which pertains the 4-aminophenolate (4AP*) (**Figure 9F**) and visually displays a color change from bright yellow to clear. The result indicates that all three catalysts aided in the breakdown of $NaBH_4$, both

providing a hydrogen source on the surface of the catalyst for the reduction of 4NP*, as well as giving off excess hydrogen gas. The gas production is seen on the UV-Vis spectra by an increased baseline and perturbation (**Figure 9D**). To monitor the reduction of at λ_{max} = 400 nm for the kinetics, each spectrum was normalized using an isosbestic point of 250 nm.

Utilizing the pseudo-first order kinetics equation, the rates of reduction were obtained (**Figure 9F**) and found to be in the order of Co_{100}(0.189 min^{-1}) > Co_{350}(0.057 min^{-1}) > Co_{600}(0.033 min^{-1}). The Co_{350} species is likely the highest performing due to its composition being mainly Co_3O_4 but having more defects and oxygen vacancies than the Co_{600} which was more crystalline. The reason Co_3O_4 is a better catalyst for this reduction was presented by Chen et al. who reported that oxygen vacancy in Co_3O_4 provides enhanced activity of 4NP reduction whereas crystalline Co_3O_4 showed no reactivity for the first 30 min[25]. This reasoning explains why the Co_{600}, which had a more crystalline structure than Co_{350}, had a slower rate of reduction as well as smaller surface area.

Comparing different catalysts through the reduction of 4NP is difficult due to the amount the variables such as stirring rate and time, concentration of reactions, volume, temperature, amount of catalyst used, and the nature of the catalysts such as active sites, surface area, and composition. However, it is accepted that k_{app} as a function of catalyst mass and reaction volume is an acceptable method of comparing different catalysts' activities. This value is called the "activity parameter" and is labeled as κ ($s^{-1}g^{-1}L$). Using this standard, our highest performing

catalyst, Co_{350}, has a κ value of 9.5 x 10^{-3} $s^{-1}g^{-1}L$. This activity parameter is similar to SiO2@Ag-Au particles produced by Wang et al[26]. These had an κ value of 16.907 x 10^{-3} $s^{-1}g^{-1}L$. Composite polyhedron particles (Co_3O_4/CoP), discussed in the Literature Review, produced by Shi-Zhao Kang[5] had a higher activity parameter of 0.298 $s^{-1}g^{-1}L$ but were synthesized through an extensive wet chemistry technique that took well over 40 hr.

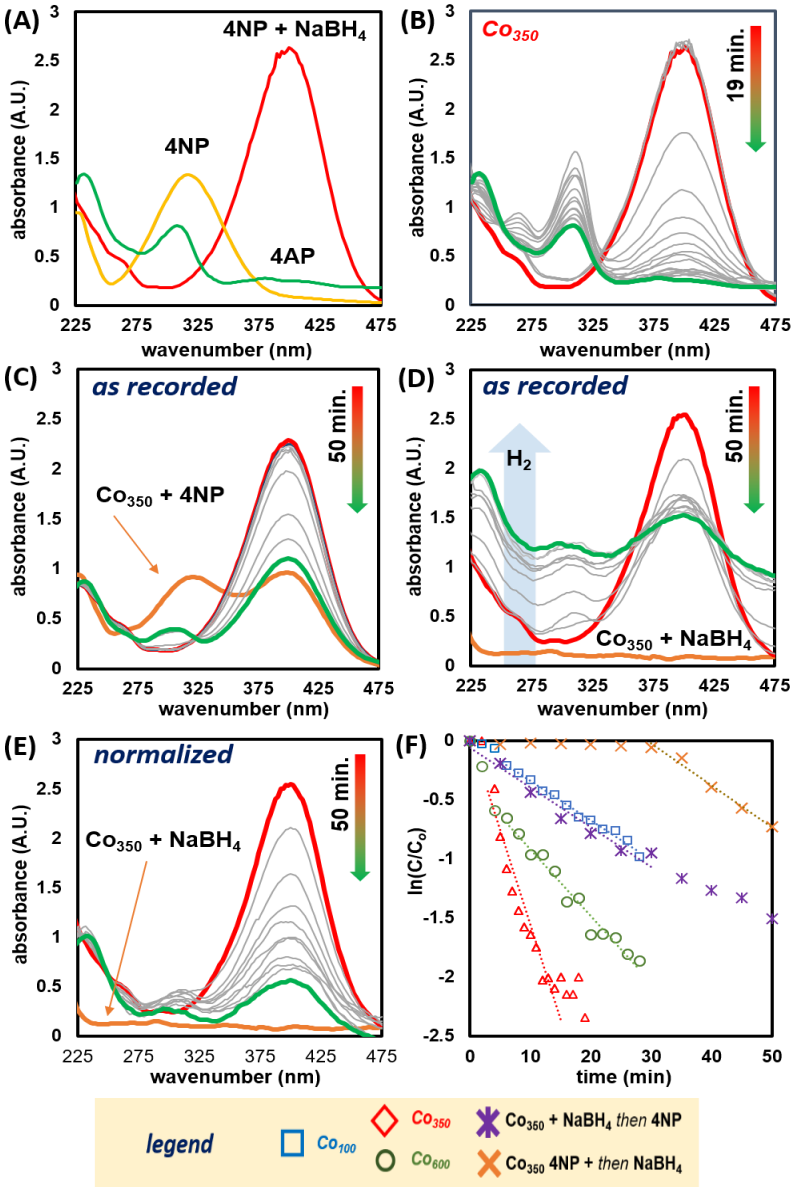

Figure 9: Catalysis Trials

Comparing different catalysts through the reduction of 4NP is difficult due to the amount the variables such as stirring rate and time, concentration of reactions, volume, temperature, amount of catalyst used, and the nature of the catalysts such as active sites, surface area, and composition. However, it is accepted that k_{app} as a function of catalyst mass and reaction volume is an acceptable method of comparing different catalysts' activities. This value is called the "activity parameter" and is labeled as κ ($s^{-1}g^{-1}L$). Using this standard, our highest performing catalyst, Co_{350}, has a κ value of 9.5 x 10^{-3} $s^{-1}g^{-1}L$. This activity parameter is similar to SiO_2@Ag-Au particles produced by Wang et al[26]. These had an κ value of 16.907 x 10^{-3} $s^{-1}g^{-1}L$. Composite polyhedron particles (Co_3O_4/CoP) dicussed in the Literature Review produced by Shi-Zhao Kang[5] had a higher activity parameter of 0.298 $s^{-1}g^{-1}L$ but were synthesized through an extensive wet chemistry technique that took well over 40 hr.

Additional catalysis experiments were performed to examine the mechanism of reduction. Two of these experiments were to determine whether the order in which the reactants were introduced in the system would impact the reduction rate. The first such experiment consisted of Co_{350}, 4NP, and water being put into the system and obtaining an initial measurement before adding $NaBH_4$ and monitoring the kinetics (**Figure 9D**). The initial scan in this experiment displayed a red shift without the presence $NaBH_4$ due to the presence of residual KOH on the catalyst surface. After an induction time of 30 min, the reaction proceeded at a rate of 0.032 min^{-1}. The second experiment consisted of Co_{350}, $NaBH_4$, and water being the system for the initial scan and then adding 4NP to monitor the kinetics (**Figure 9E**). There was only an induction period

of about 5 min before this reaction then proceeded at a rate of 0.035 min^{-1}. Both reductions occurred at a slower rate than the original order of testing Co_{350}, which had 4NP, $NaBH_4$, and water introduced for the initial scan and adding the catalyst last to monitor kinetics. This slower rate of the varied order lends trust to the Langmuir-Hinshelwood mechanism model because the adsorption constant of Co_3O_4 for 4NP is higher than BH_4^- (K_{4NP}=922$\pm$40 L mol^{-1} and K_{BH4}-=22 $\pm$4 L mol^{-1}). This explains why the induction period of the first experiment was considerably longer than that of the second. As 4NP has a higher affinity to the catalyst than the BH_4^-, it took longer for the desorption of 4NP and thus to create room for the BH_4^- to adsorb on the catalyst surface for the Langmuir-Hinshelwood mechanism to occur.

The pH and temperature of the reduction was also monitored for mechanistic studies. The pH of the system shows an initial drop likely due to some of the BH_3^- adsorbing onto the catalyst surface. It further shows a quick increase of pH and then tapers off. This increase and leveling is likely due to the hydrolysis of $NaBH_4$ producing borate (BO_3^{3-}) (**Figure 10A**). The temperature proves to be fairly constant, remaining between 20.5 ˚C and 21.6 ˚C (**Figure 10B**).

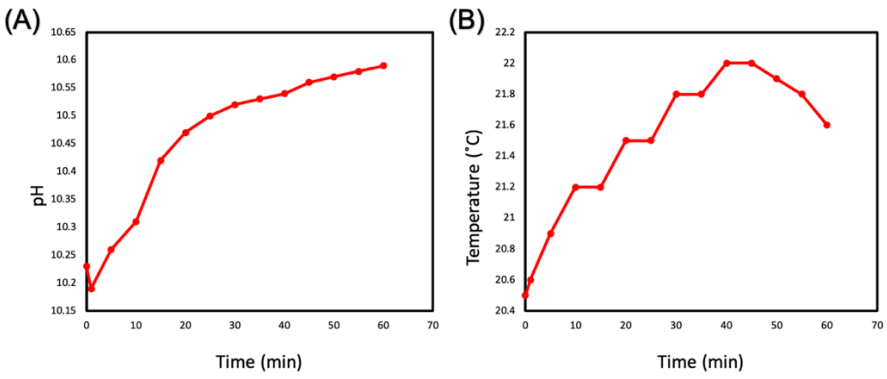

Figure 10: pH (A) and Temperature Experiments (B)

Finally, pressure was investigated by comparing two experiments. The first experiment introduced 0.2 mmol of $NaBH_4$ in 3 mL of DIW and 1 mg of the catalyst in a sealed vial and measured the change in pressure. Because this is an isothermal and isochoric process, the change in pressure can be related to the number of moles of hydrogen gas produced by utilizing the Van der Waals Equation for non-ideal gases. Using this model, the amount of hydrogen gas produced was 0.238 mmol (**Figure 11A**). A similar experiment with 0.2 mmol of $NaBH_4$ and 0.39 µmol of 4NP in 3 mL of DIW and 1 mg of catalyst was monitored for the pressure change (**Figure 11B**). Using the Van der Waals equation, the amount of hydrogen gas was 0.159 mmol. The decrease in hydrogen gas produced in the presence of 4NP can be explained by the fact that the hydrogen produced from the catalytic hydrolysis of $NaBH_4$ was used for the reduction of 4NP* and thus not expelled as gas. This can also be seen in the shape of the graphs. In absence of 4NP, the pressure increases with a logarithmic shape, thus indicating quick production of hydrogen gas, whereas in the presence of 4NP the graph has an exponential plot. This is likely due to the initial hydrolysis of $NaBH_4$ being used for the reduction of 4NP* and once this is complete, the hydrogen produced is expelled as gas, thus increasing pressure.

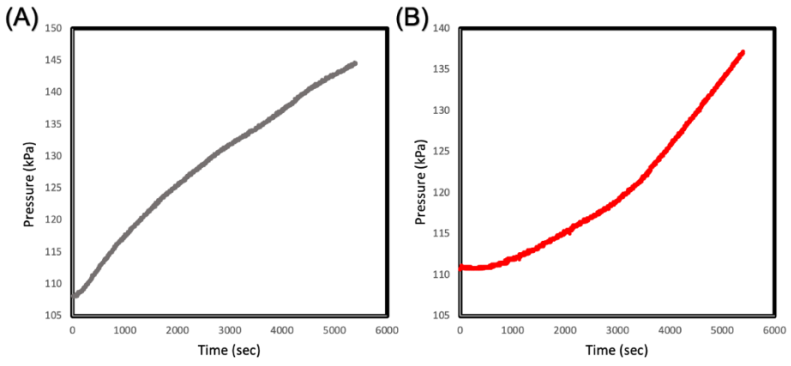

Figure 11: Pressure of System in Absence of 4NP (A) and in Presence of 4NP (B)

3.3: Investigation of KOH Impact on Reduction

Residual KOH from the ball-milling synthesis was detected in the Raman spectroscopy, FTIR, and the red shift of the 4NP species in the presence of only DIW and Co_{350}. In order to determine the impact of the KOH on the catalytic reduction of 4NP, several experiments were conducted. Firstly, a system of 0.39 µmol 4NP and 0.2 mmol $NaBH_4$ in 3 mL of DIW was studied with the addition of 1 mg of KOH instead of the 1 mg of cobalt catalyst. This system was monitored identically to the prior catalysis tests. This experiment resulted in no change in the 4NP* peak or any appearance of the 4AP* peak after 28 min (**Figure 12A**). Secondly, the catalytic reduction of 4NP using Co_{350} was conducted with the addition of 1 mg of KOH (**Figure 12C**). This produced a slower rate of 0.132 min^{-1} as opposed to the 0.189 min^{-1} rate in the absence of additional KOH. The UV-Vis spectrum displays a marked increase in λ_{max} = 310 nm. However, the addition of 1 mg of KOH to 4AP results in the 4AP* peak absorbance increase of only Δ 0.03 a.u. over 28 min (**Figure 12D**). Thus, the formation of K^+AP* is not a sufficient explanation for the dramatic increase of absorbance at this wavelength.

A viable explanation of the increase at λ_{max} = 310 nm is that the KOH could be providing an alternate pathway for the reduction of 4NP. This was first presented by Yan, Xie et al. who proposed the direct hydrogenation of 4NP to form 4-nitrosophenol which yields 4AP/4AP*[27]. Thus, the increased concentration of K^+ may provide a complementary reduction pathway through 4-nitrosophenol which accounts for the increased absorbance and slightly slower rate of

reduction. Overall, it is clear that the residual KOH in the system is not the catalytic driving force for the reduction of 4NP.

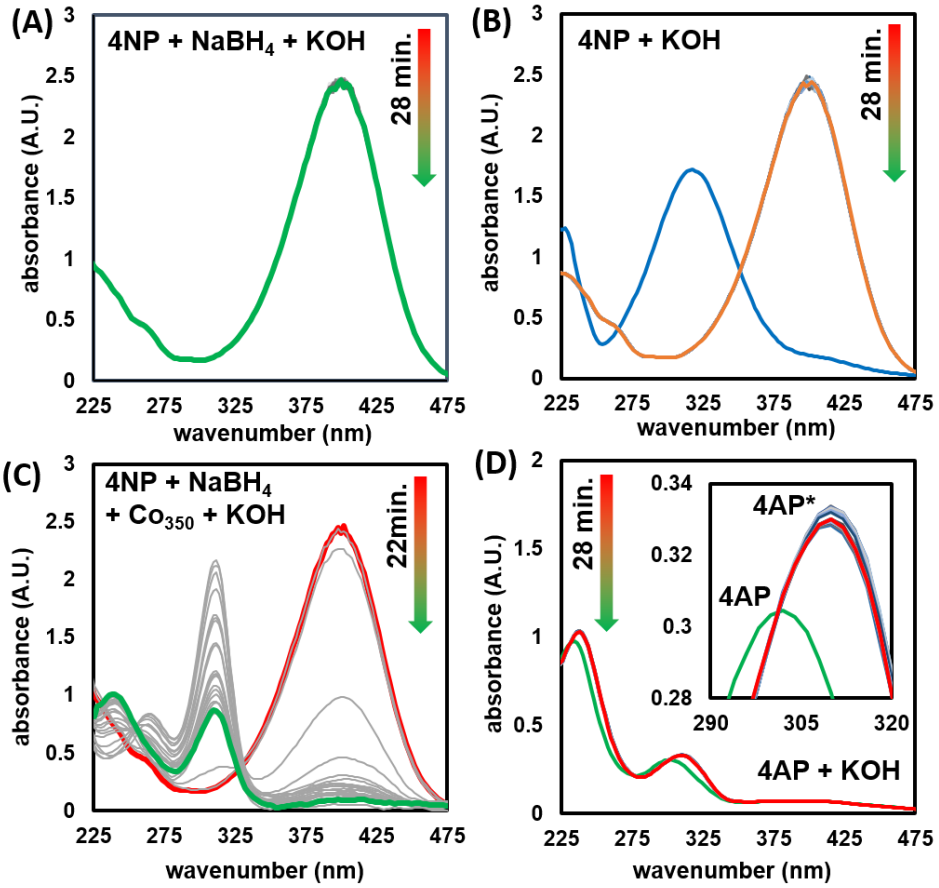

Figure 12: Investigation of KOH

3.4: Recyclability of Co_{350}

Recyclability of catalysts is a vital property as it pertains to cost-efficiency and broad-scope application of the catalysts. The recyclability of the Co_{350} catalyst was investigated using identical conditions as the catalytic tests of 4NP. Initially, this species was exposed to ambient conditions of 45-55 % humidity which decreased the rate by 48 % to 0.091 min^{-1}. This is likely due to H_2O and CO_2 adsorbing onto the catalyst surface both blocking active sites as well as lowering the

catalyst weight percent in the measured 1 mg of compound for the trial. After the initial trial, four additional trials were performed over the span of 9 days (**Figure 13**). Between each trial the solution was allowed to settle and carefully decanted. The remaining particles were rinsed with DIW and dried in a vacuum oven. Over the total 5 trials, the k_{app} rate reduced by a further 21 %. This may be due to catalyst degradation but is likely due to mechanical loss during workup. The fluctuation of rate between each trial is likely due to agglomeration and dispersion of particles.

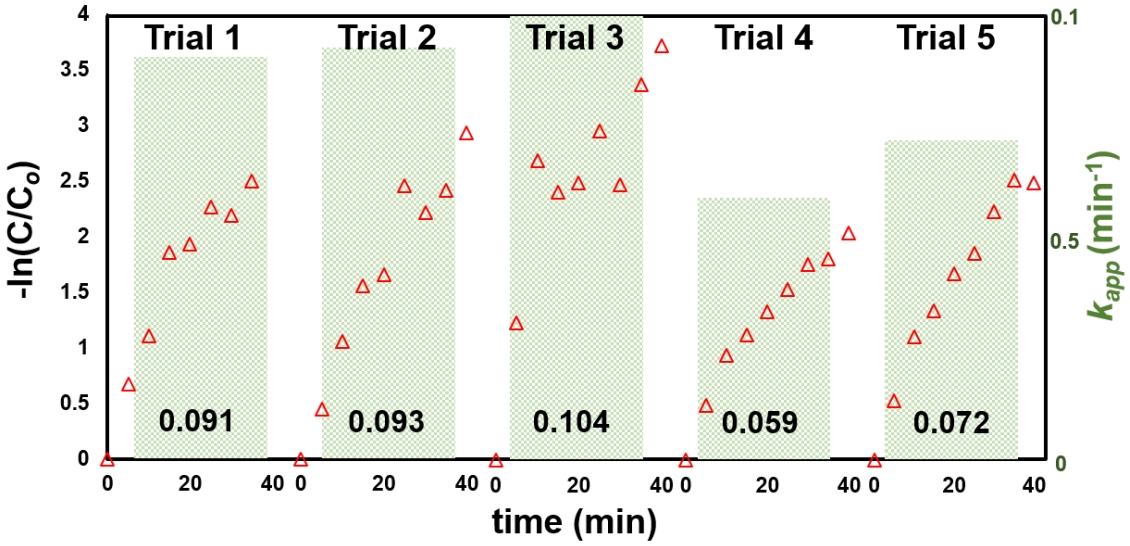

Figure 13: Recyclability of Co_{350}

3.5: Catalytic Reduction of Substituted Nitrophenols

Although the reduction of 4NP has been considered a "model reaction" when it comes to comparing the activity of catalysts, just using the reduction of 4NP could potentially overlook more active or selective catalysts. For this reason, the cobalt oxide-based particles synthesized were tested for the reduction of two substituted nitrophenols as well, namely: 4-amino-3-nitrophenol (4A5NP) and 2-amino-5-nitrophenol (2A5NP). The setup was identical to the catalytic

tests of 4NP, however the wavelength degradation monitored was λ_{max} = 510 nm for 4A3NP and λ_{max} = 460 nm for 2A5NP. Notably, both species in the presence of $NaBH_4$ produced a red shift in the UV-Vis spectra corresponding to their respective deprotonated phenolate species (**Figure 14A and Figure 14D**). The reduction of 4A3NP was fastest with the Co_{350} catalyst, giving a k_{app} = 0.114 min^{-1} (**Figure 14B and Figure 14C**), while that of Co_{100} and Co_{600} produced only slight activity with k_{app} = 0.004 and 0.003 min^{-1} respectively.

Interestingly, the reduction of 2A5NP using Co_{100} produced two distinct rates after an induction period of 8 min. The first k_{app} was a modest 0.047 min^{-1} but after 26 min the k_{app} increased to 0.175 min^{-1} (**Figure 14F**). This is likely due to the multi-component composition of Co_{100} whereas the CoO(OH) and $Co(OH)_2$ species could provide the initial rate while the Co_3O_4 species could provide the increased second rate of reduction. Use of Co_{600} provided k_{app} = 0.264 min^{-1} after an induction period of 22 min while Co_{350} provided this slowest k_{app} = 0.143 min^{-1} (**Figure 14E**). The order of these rates is inversely proportional to the BET surface area of these catalysts (Co_{350} = 28.28 m^2g^{-1} and Co_{600} = 10.38 m^2g^{-1}) and thus is likely attributed to the nature of available surface sites as determined by the particle size and crystallinity.

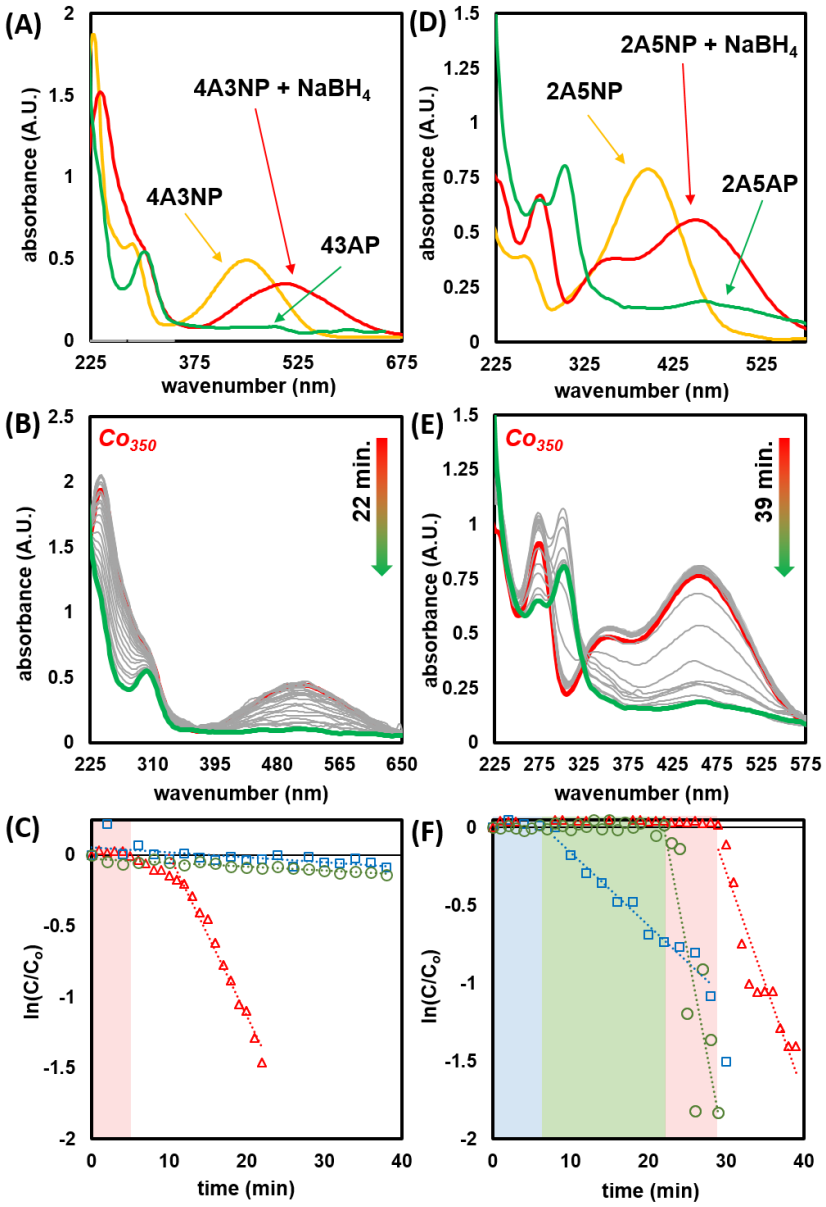

Figure 14: Reduction of 4A3NP and 2A5NP

3.6: Application of Reduction in a Flow Process

In order to investigate the application of this reduction in a real-world system, a proof-of-concept model was used. For this, 12 mg of Co_{350} was loaded into two 0.22 µm nylon syringe filters (8 mg

in filter i and 4 mg in filter ii) and stacked on a luer-lock syringe. The syringe was filled with 48 mL of DIW solution including 6.21 µmol 4NP and 3.2 mmol $NaBH_4$ (**Figure 15**). This solution was flowed through the filters at a rate of 0.4 mL min^{-1} and the product was collected and analyzed through UV-Vis spectrophotometry. This spectrum not only displayed this complete disappearance of λ_{max} = 400 nm pertaining to the 4NP* but also the appearance of λ_{max} = 300 nm which corresponds to 4AP as opposed to the 4AP* peak observed for the in-situ trials discussed prior.

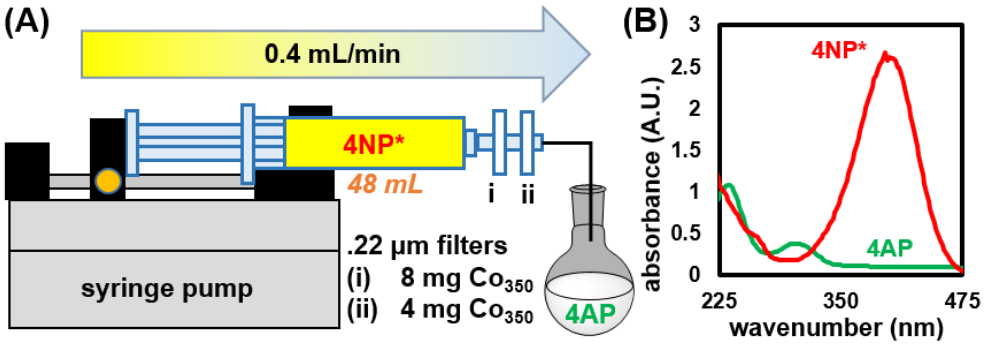

Figure 15: Flow Process Set-Up

CHAPTER 4: CONCLUSIONS

Reduction of nitrophenols is not only an important approach to provide a scientific method of comparing catalysts but also a vital reduction for the remediation of toxic environmental contaminants. Providing sustainable catalysts that work in a flow process for this reduction is advantageous for the potential application in larger water remediation systems. Likewise, better understanding of the mechanism and system of the catalytic reduction of nitrophenols is vital if furthering this science is to be possible. Presented, cobalt oxide-based particles were synthesized in a facile, green method that provided sustainable catalysts for the reduction of at least three unique nitrophenols. Finally, these particles proved adaptable to a flow process and provided reliable recyclability.

REFERENCES

1. Podeh, M. R.; Bhattacharya, S. K.; Qu, M. Water Research 1995, **29** (2), 391–399.

2. Park, J.; Bae, S. Chemosphere 2018, **202**, 733–741.

3. Keith, L.; Telliard, W. Environmental Science & Technology 1979, **13** (4), 416–423.

4. Aditya, T.; Pal, A.; Pal, T. ChemInform 2015, **46** (29).

5. Liu, X.; Li, X.; Qin, L.; Mu, J.; Kang, S.-Z. Applied Surface Science 2018, **434**, 967–974.

6. Shah, D.; Kaur, H. Journal of Molecular Catalysis A: Chemical 2014, **381**, 70–76.

7. Dolatkhah, A.; Jani, P.; Wilson, L. D. Langmuir 2018, **34** (36), 10560–105688.

8. Pandey, S.; Mishra, S. B. Carbohydrate Polymers 2014, **113**, 525–531.

9. Mei, Y.; Sharma, G.; Lu, Y.; Ballauff, M.; Drechsler, M.; Irrgang, T.; Kempe, R. Langmuir 2005, **21** (26), 12229–12234.

10. Gopalakrishnan, R.; Loganathan, B.; Dinesh, S.; Raghu, K. Journal of Cluster Science 2017, **28** (4), 2123–2131.

11. Wunder, S.; Polzer, F.; Lu, Y.; Mei, Y.; Ballauff, M. The Journal of Physical Chemistry C 2010, **114** (19), 8814–8820.

12. Mogudi, B. M.; Ncube, P.; Meijboom, R. Applied Catalysis B: Environmental 2016, **198**, 74–82.

13. Gopiraman, M.; Deng, D.; Saravanamoorthy, S.; Chung, I.-M.; Kim, I. S. RSC Advances 2018, **8** (6), 3014–3023.

14. Ghosh, S.; Mandal, M.; Kundu, S.; Nath, S.; Pal, T. Applied Catalysis A: General 2004, **268** (1-

2), 61–66.

15. Mandlimath, T. R.; Gopal, B. Journal of Molecular Catalysis A: Chemical 2011, **350** (1-2),9-15.

16. Zheng, C.; Cao, C.; Ali, Z.; Hou, J. J. Mater. Chem. A 2014, 2 (39), 16467–16473.

17. Liu, B.; Zhang, X.; Shioyama, H.; Mukai, T.; Sakai, T.; Xu, Q. Journal of Power Sources 2010, 195 (3), 857–861.

18. Nguyen, T.; Boudard, M.; Rapenne, L.; Chaix-Pluchery, O.; Carmezim, M. J.; Montemor, M. F. RSC Advances 2015, 5 (35), 27844–27852.

19. Liu, Y.-C.; Koza, J. A.; Switzer, J. A. Electrochimica Acta 2014, 140, 359–365.

20. Alrehaily, L. M.; Joseph, J. M.; Wren, J. C. Physical Chemistry Chemical Physics 2015, 17 (37), 24138–24150.

21. Li, N.; Zhu, Y. D.; Liu, T.; Liu, S. G.; Lin, S. M.; Shi, Y.; Luo, H. Q.; Li, N. B. New Journal of Chemistry 2017, 41 (5), 1993–1996.

22. Nie, Q.; Cai, Q.; Xu, H.; Qiao, Z.; Li, Z. Analytical Methods 2018, 10 (22), 2623–2628.

23. George, G.; Anandhan, S. RSC Advances 2015, 5 (99), 81429–81437.

24. Rouquerol, F.; Rouquerol, J.; Sing, K. Adsorption by powders and porous solids: Principles, methodology and applications; Academic Press: San Diego, 1999.

25. Kong, X.-K.; Sun, Z.-Y.; Chen, M.; Chen, C.-L.; Chen, Q.-W. Energy & Environmental Science 2013, 6 (11), 3260.

26. An, Q.; Yu, M.; Zhang, Y.; Ma, W.; Guo, J.; Wang, C. The Journal of Physical Chemistry C 2012, 116 (42), 22432–22440.

27. Nasaruddin, R. R.; Yao, Q.; Chen, T.; Hülsey, M. J.; Yan, N.; Xie, J. Nanoscale 2018, 10 (48), 23113–23121.